AN ANALYTIC SOLUTION TO THE FÖRSTER ENERGY TRANSFER PROBLEM IN TWO DIMENSIONS

PAUL K. WOLBER AND BRUCE S. HUDSON, *Department of Chemistry, Stanford University, Stanford, California 94305 U.S.A.*

ABSTRACT An analytic solution of the Förster energy transfer problem in two dimensions is presented for the case in which the orientation factor is independent of the donor-acceptor distance, and both the donors and acceptors are randomly distributed in a plane. A general solution based on the method of Förster is possible since all distances are measured in units of R_0. The analytic solution is extended to the cases of donors embedded in structures that exclude acceptors, and donors that bind acceptors. The validity of the analytic solutions is demonstrated by comparison with numerical simulation calculations. Numerical approximations to the exact solutions are given for ease of computation. Specific applications to the case of fluorescence quenching of a membrane-bound donor by membrane-bound acceptors are presented.

INTRODUCTION

The problem of energy transfer in two dimensions is of interest because of its relevance to the analysis of fluorescence quenching experiments in which both the donor and acceptor are bound to a lipid bilayer membrane. Membrane fusion, protein-protein association, lipid-protein interaction, lipid lateral phase separations, and bilayer spacing can all be studied by energy transfer. A typical example is the quenching of the fluorescence of a randomly distributed donor (e.g., a tryptophan residue or a fluorescent label on a protein or a lipid component of the bilayer) due to the addition of an acceptor to the membrane. The solution of this problem for the laterally static, random distribution case forms the necessary background for the evaluation of the effects of diffusion and nonrandom distributions on the efficiency of energy transfer.

This problem has recently been treated by Fung and Stryer (1), who presented numerical solutions for specific values of the 50% energy transfer distance, R_0, and a specific value of the area per lipid molecule in a bilayer. In this paper we show that the method used by Förster for the corresponding three-dimensional problem (2) may be used to obtain an exact analytic solution for the transfer efficiency in the form of a rapidly converging series expansion that is valid for all values of R_0 and all values of the area per lipid molecule in the membrane. The analytic solution agrees well with a direct simulation of the problem, and is approximated by an easily computed sum of two exponentials. The cases in which acceptors are excluded from a region surrounding each donor or are bound to the donors are treated.

Dr. Hudson's present address is Department of Chemistry and Institute of Molecular Biology, University of Oregon, Eugene, Oreg. 97403.

Calculated and Measured Quantities Related to Nonradiative Energy Transfer

The fundamental effect of nonradiative energy transfer from a fluorescent donor to randomly distributed acceptors is to induce a multiplicity of donor molecule environments. Donors in these different environments experience different rates of nonradiative quenching, with the result that the fluorescence decay function calculated or measured for an ensemble of donors is nonexponential, even though the decay functions for individual environments within the ensemble are exponential. An analytic form for such an ensemble decay function was first derived by Förster (2) for nonradiative transfer in solution, and has been elaborated upon by Eisenthal and Siegel (3). Fluorescence decays in such systems are directly measurable by pulse fluorometry.

The quantum yield for an ensemble of statically illuminated donor molecules is calculable from the fluorescence decay function. Let $P(t - t')\,dt'$ denote the probability that a donor excited at time t' is still excited at time t, $P(0) = 1$. Then the quantum yield q measured in a static fluorescence experiment is given by

$$q = \frac{\int_{-\infty}^{t} P(t - t')\,dt'}{\int_{-\infty}^{t} P_0(t - t')\,dt'} = \frac{\int_{0}^{\infty} P(t')\,dt'}{\int_{0}^{\infty} P_0(t')\,dt'}, \tag{1}$$

where $P_0(t - t')$ is the probability density function analogous to $P(t - t')$ when only radiative de-excitation of the donors occurs.

Analytic Theory

An analytic theory of nonradiative energy transfer by the Förster mechanism to acceptors randomly placed in two dimensions may be derived in a manner analogous to that in three dimensions, provided that the following assumptions are met: (*a*) The donor and acceptor concentrations are low enough that the steady-state (or transient) concentration of excited donors is much less than the concentration of acceptors, and that the area contributed by donors and acceptors is negligible (no excluded area effects). (*b*) R_0 is not a function of R_i, the distance between a given donor and A_i, the i^{th} acceptor surrounding it. (*c*) the orientation dependence implicit in R_0 is not time-dependent on the time scale of the fluorescence lifetime, i.e., either the dynamic or static averaging limit holds (4). (*d*) The distance of closest approach between donor and acceptor, R_e, is much less than R_0.

By assumption (*a*), we need only consider one donor molecule. Let the lifetime of an excited donor D^* in the absence of acceptors $\{A_i\}$ be denoted by τ. If one considers a finite disk of radius R_d surrounding D^*, containing $\{A_i\}$ at distances $\{R_i\}$, the rate of de-excitation is given by (2, 3)

$$k = \tau^{-1}\left[1 + \sum_{i=1}^{N} (R_0/R_i)^6\right],$$

for nonradiative transfer by a weak dipole-dipole coupling (Förster) mechanism. N denotes the number of acceptor molecules found in the disk, and must satisfy the relationship

$$N = \pi R_d^2 c, \tag{2}$$

where c is the two-dimensional concentration of acceptors (per unit area).

Since all of the de-excitation pathways are first order in the excited donor concentration, the probability density $P(t)$ for D^* still being excited after time t must satisfy the differential equation

$$-\frac{\mathrm{d}}{\mathrm{d}t}P(t) = kP(t) = \tau^{-1}\left[1 + \sum_{i=1}^{N}(R_0/R_i)^6\right]P(t), \tag{3}$$

with the initial condition P(0) = 1. Eq. 3 is easily integrated to yield

$$P(t) = e^{-t/\tau}\prod_{i=1}^{N}\exp\left[-(t/\tau)(R_0/R_i)^6\right]. \tag{4}$$

The ensemble average decay function in a finite disk, $<P(t)>_N$, is therefore given by

$$<P(t)>_N = e^{-t/\tau}\prod_{i=1}^{N}\int_0^{R_d}\exp\left[-(t/\tau)(R_0/R_i)^6\right]W(R_i)\,\mathrm{d}R_i, \tag{5}$$

where $W(R_i)\,\mathrm{d}R_i$ is the probability of finding acceptor A_i in the annulus between radii R_i and $R_i + \mathrm{d}R_i$, $\int_0^{R_d} W(R_i)\,\mathrm{d}R_i = 1$, assumption (a) has been used to factor the terms $W(R_i)\,\mathrm{d}R_i$ into individual integrals, and assumption (d) has been used to set the lower limit of the integral in Eq. 5 equal to zero.

Eq. 5 may be simplified considerably by noting that to say that the donors are randomly distributed is to say that the functions $W(R_i)$ are identical for all values of i. Therefore, the integrals in the product are all identical. With the definition

$$J(t) = \int_0^{R_d}\exp\left[-(t/\tau)(R_0/R)^6\right]W(R)\mathrm{d}R, \tag{6}$$

Eq. 5 becomes

$$<P(t)>_N = e^{-t/\tau}[J(t)]^N. \tag{7}$$

For a random, planar system,

$$W(R)\,\mathrm{d}R = \frac{2R\mathrm{d}R}{R_d^2}.$$

After the substitution $\chi = (R_0/R)^6(t/\tau)$ and the definition

$$\chi_d = (R_0/R_d)^6(t/\tau) \tag{8}$$

Eq. 6 becomes

$$J(t) = \frac{1}{3}\chi_d^{1/3}\int_{\chi_d}^{\infty}\chi^{-4/3}e^{-\chi}\,\mathrm{d}\chi. \tag{9}$$

Integration of Eq. 9 by parts produces

$$J(t) = e^{-\chi_d} - \chi_d^{1/3}\,\Gamma(2/3) + \chi_d^{1/3}\int_0^{\chi_d} \chi^{-1/3} e^{-\chi}\,d\chi, \tag{10}$$

where

$$\Gamma(x) = \int_0^{\infty} y^{x-1} e^{-y}\,dy. \tag{11}$$

In the limit of large N, and therefore large R_d and small χ_d, only the lowest order terms in χ_d will be important. Expanding the exponential and integral in Eq. 10 as power series, and keeping only terms up to $0(\chi_d^{1/3})$, one obtains

$$J(t) \approx 1 - \Gamma(2/3)\chi_d^{1/3}. \tag{12}$$

Combination of Eqs. 12, 8, 7, and 2 produces

$$<P(t)>_N = e^{-t/\tau}\left[1 - \frac{\pi\Gamma(2/3)R_0^2 c}{N}(t/\tau)^{1/3}\right]^N.$$

The desired decay function is $<P(t)> = \lim_{N\to\infty} <P(t)>_N$. By using the relationship

$$\lim_{N\to\infty}(1 + a/N)^N = e^a,$$

we obtain the result,

$$<P(t)> = \exp\left[-(t/\tau) - \pi\Gamma(2/3)R_0^2 c(t/\tau)^{1/3}\right]. \tag{13}$$

The notation of Eq. 13 may be simplified by means of two substitutions. Let

$$\epsilon = \pi\Gamma(2/3) \approx 4.25409,$$

$$C = R_0^2 c.$$

C is the concentration of acceptors per R_0^2, the "natural" concentration for this problem. Eq. 13 now becomes (5, 6)

$$<P(t)> = \exp\left[-(t/\tau) - \epsilon C(t/\tau)^{1/3}\right]. \tag{14}$$

The ratio of the donor quantum yields in the presence and absence of acceptors, $q_{D(A)}$ and q_D, may now be calculated from Eq. 1 by noting that, in the absence of acceptors,

$$P(t)dt = e^{-t/\tau}dt.$$

Making the definition $\lambda = t/\tau$, one obtains

$$q_r = q_{D(A)}/q_D = \int_0^{\infty} e^{-\lambda} e^{-\epsilon C\lambda^{1/3}}\,d\lambda. \tag{15}$$

The relative quantum yield q_r is related to the transfer efficiency E by $E = 1 - q_r$. Eq. 15 may be evaluated by expanding $e^{-\epsilon C\lambda^{1/3}}$ as a power series and by using Eq. 11 to integrate term by

term, to yield

$$q_r = \sum_{j=0}^{\infty} [(-\epsilon C)^j \Gamma(j/3 + 1)/j!]. \tag{16}$$

A graph of q_r as a function of C is presented in Fig. 1. The integration in Eq. 15 has also been performed by a fifteen point Laguerre procedure (7), and the results are also shown in Fig. 1.

The series in Eq. 16 is an alternating series of terms that decreases rapidly with j beyond some critical value of j. Because of the alternation in sign, the difference between a given partial sum and the limit sum decreases monotonically with j, once the terms in the sum start decreasing monotonically with j. Under these conditions any two consecutive partial sums bracket the limit sum, and thus provide rigorous upper and lower bounds to the exact result.

Note that Eqs. 14 and 16 are valid for any donor-acceptor system in a plane satisfying assumptions (*a*)–(*d*). The particular value of R_0 for the system has been incorporated into a decreasing monotonically with j. Under these conditions any two consecutive partial sums bracket the limit sum, and thus provide rigorous upper and lower bounds to the exact result.

Note that Eqs. 14 and 16 are valid for any donor-acceptor system in a plane satisfying assumptions (*a*)–(*d*). The particular value of R_0 for the system has been incorporated into a scaling factor for the concentration, and does not enter into the calculation of the quenching curve. The expression of the model parameters in terms of dimensionless numbers represents an important simplification of any energy transfer problem, a simplification that must be made before the effects of changes in the assumptions behind the model can be evaluated clearly.

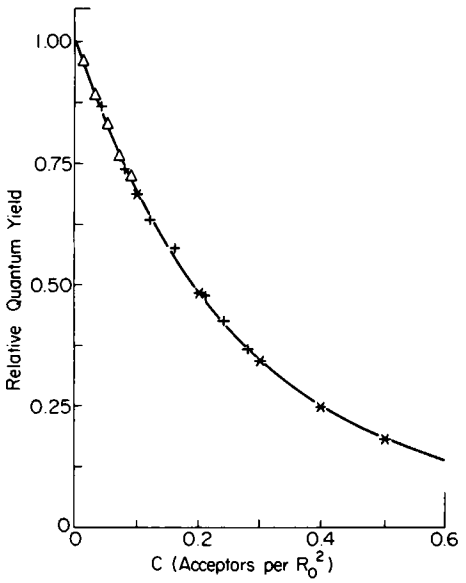

FIGURE 1 Quenching of randomly distributed donors by randomly distributed acceptors: prediction of Eq. 16 (—); computer simulation, $[D] = 0.1$ per R_0^2 (△); computer simulation, $[D] = 0.5$ per R_0^2 (+); approximate form, Eq. 17 (*). $[D]$ is the concentration of donors.

TABLE I
NUMERICAL FIT TO
QUENCHING CURVES

R_e/R_0	A_1	k_1	A_2	k_2
0.0	0.6463	4.7497	0.3537	2.0618
0.25	0.6290	4.5752	0.3710	1.9955
0.5	0.6162	4.0026	0.3838	1.4430
0.7	0.6322	3.1871	0.3678	0.7515
0.8	0.6344	2.7239	0.3656	0.4706
0.9	0.6336	2.2144	0.3664	0.2909
1.0	0.6414	1.7400	0.3586	0.1285
1.1	0.6327	1.3686	0.3673	0.4654
1.3	0.6461	0.4899	0.3539	0.5633

Fit parameters for use in Eq. 17. The approximations were generated by a nonlinear least-squares fit on 50 points generated by Eq. 22, for C in the range between 0.0 and 0.6.

A convenient approximation to Eq. 16, accurate to better than 1% for $0 \leq C \leq 0.5$, is given by

$$q_r \approx A_1 e^{-k_1 C} + A_2 e^{-k_2 C}, \tag{17}$$

where A_1, k_1, A_2, and k_2 are given in Table I.

Analytic Theory when R_e is Comparable to R_0

As an illustration of the general applicability of the approach presented in the previous section, we calculate an analytic form for $<P(t)>$ when assumption (d) does not hold, in particular when the distance of closest approach, R_e, is of the order of R_0. This more general case is meant to model such systems as a tryptophan donor protected from acceptors dissolved in the host lipid by a shell of surrounding protein or boundary lipid.

Three key changes in the previous treatment are required. Eq. 6 now reads

$$J(t) = \int_{R_e}^{R_d} \exp\left[-(t/\tau)\,(R_0/R)^6\right] W(R)\,\mathrm{d}R \tag{18}$$

and, in order that $W(R)$ remain normalized,

$$W(R)\,\mathrm{d}R = 2R\mathrm{d}R/(R_d^2 - R_e^2).$$

Finally, N now satisfies

$$c = N/[\pi(R_d^2 - R_e^2)]. \tag{19}$$

The integration by parts and truncation proceed exactly as before, except that now we make use of the incomplete gamma function,

$$\gamma(x, y) = \int_0^y z^{x-1} e^{-z}\,\mathrm{d}z, \tag{20}$$

to obtain

$$\langle P(t)\rangle = \exp\{-(t/\tau) - \pi R_0^2 c\gamma[2/3, (R_0/R_e)^6(t/\tau)](t/\tau)^{1/3} + \pi R_e^2 c[1 - e^{-(R_0/R_e)^6(t/\tau)}]\}. \quad (21)$$

The effect of a nonnegligible value of R_e has been to produce a time-dependent scaling of ϵ in Eq. 14. Since $\gamma(x,y) < \Gamma(x)$ and the term in $R_e^2 c$ is greater than zero, this scaling depresses the apparent acceptor concentration from that in Eq. 14 and, therefore, the quenching.

The relative quantum yield q_r may be calculated in a manner analogous to that in Eq. 15. Defining λ and C as before, and letting

$$\alpha = (R_e/R_0)^6,$$

the relative quantum yield is given by

$$q_r = \int_0^\infty e^{-\lambda} \exp[-\pi C\gamma(2/3,\lambda/\alpha)\lambda^{1/3}] \exp[\pi C\alpha^{+1/3}(1 - e^{-\lambda/\alpha})]d\lambda. \quad (22)$$

Because of the λ dependence of $\gamma(2/3,\lambda/\alpha)$ and $e^{-\lambda/\alpha}$, the integral is best done numerically. We have performed the integration by a fifteen point Laguerre procedure, and the results are summarized in Fig. 2, along with the results of several numerical simulations.

The results of the approximation of Eq. 22 with the double exponential form of Eq. 17 are given in Table I for several values of R_e.

Analytic Solution when Donors Bind Acceptors

The form of the dependence of the relative quantum yield q_r' on acceptor concentration C in the case that one donor can bind one acceptor is easily derived from Eq. 16. The quenching in this case will consist of two parts: First, acceptors bound to donors will quench those donors with some fixed efficiency. Let the relative quantum yield of such donors be denoted $q_r^{(b)}$. In interesting cases, $q_r^{(b)}$ will be small. Second all acceptors, including those bound, will quench all donors. The relative quantum yield for such donors is given by Eq. 16. This random quenching is assumed to perturb $q_r^{(b)}$ only slightly.

The new relative quantum yield q_r' will be the weighted average of these contributions, given by

$$q_r' = f_u q_r + f_b q_r^{(b)}, \quad (23)$$

where f_u is the mole fraction of nonliganded donors, f_b is the mole fraction of liganded donors, and q_r is given by Eq. 16. f_u, f_b, q_r, and q_r' are all functions of the acceptor concentration C.

Plots of q_r' as a function of C for several donor concentrations in the extreme case that all acceptors are bound and $q_r^{(b)} = 0$ are presented in Fig. 3. Data from numerical simulations, where available, are also presented for comparison. Note that the curves even in this extreme case are nonlinear. This is due to the quenching of nonliganded donors by donor-acceptor complexes.

The modification of Eq. 23 to cover the more general case of donors that bind more than one acceptor is straightforward, but not terribly useful, since multiple binding depresses C, without much changing $q_r^{(b)}$ (since $q_r^{(b)}$ is probably already small). The effect of multiple equivalent binding sites is therefore difficult to distinguish experimentally (by means of static fluorescence experiments) from the effect of purely random quenching.

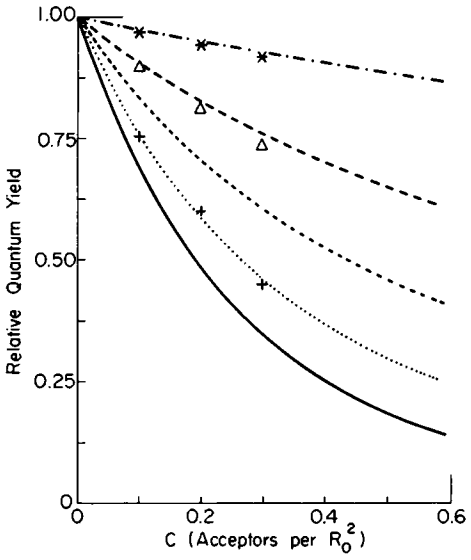

FIGURE 2

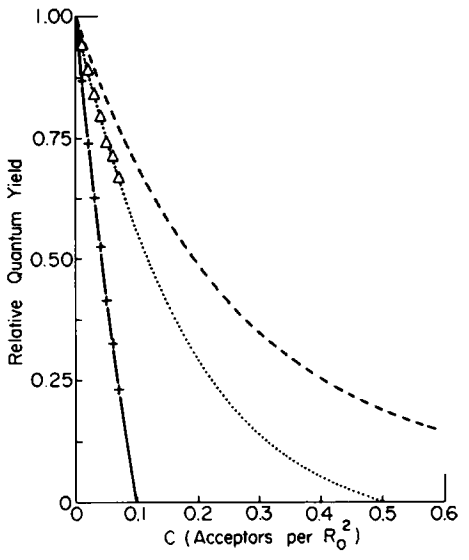

FIGURE 3

FIGURE 2 Quenching of donors that exclude acceptors, by random acceptors: nonexclusion case (—); quenching as predicted by Eq. 22 for r_D/R_0 = 0.5 (···), 0.75 (----), 1.00 (- - -), and 1.50 (-·-·); quenching from computer simulations, r_D/R_0 = 0.5(+), 1.0(△), and 1.5(∗). r_D is the donor radius, r_A/R_0 (the acceptor radius in units of R_0) is 0.05 for all cases, and $R_e = r_A + r_D$.

FIGURE 3 Quenching of donors that bind one acceptor at $R << R_0$; prediction of Eq. 23 for a donor concentration of 0.1 per R_0^2 (—) or 0.5 per R_0^2 (....); computer simulation for a donor concentration of 0.1 per R_0^2 (+), 0.5 per R_0^2 (△); curve for case of no binding (----).

Computer Simulation of Nonradiative Energy Transfer

The relative quantum yield $q_r^{(\beta)}$ for a donor surrounded by a particular configuration β of N_β acceptors is easily calculated by combining Eqs. 1 and 4:

$$q_r^{(\beta)} = \left[1 + \sum_{i=1}^{N_\beta} (R_0/R_i)^6\right]^{-1}. \tag{24}$$

The ensemble average relative quantum yield q_r may be calculated by averaging $q_r^{(\beta)}$ over a large number of acceptor configurations:

$$q_r = \lim_{M\to\infty}\left[\frac{1}{M}\sum_{\beta=1}^{M} q_r^{(\beta)}\right]. \tag{25}$$

We have performed a calculation based upon Eqs. 24 and 25 for the model system depicted in Fig. 4. The inclusion of more than one donor checks the assumption of no excluded area effects (in accordance with assumption (*a*), the calculation is done for one donor at a time, simulating a very low concentration of D^*). The inclusion of finite radii for donors and acceptors (r_D and r_A) checks assumptions (*a*) and (*d*), and prevents R_i in Eq. 24 from exactly equaling zero. Averaging only over donors in the inner box prevents edge effects. N_β is calculated from C, the acceptor concentration per R_0^2, and the area of the outer box. The

number of donors is calculated in a similar fashion, from a similarly scaled donor concentration. The parameters used in several typical simulations are summarized in Table II, along with the results and model statistics generated by these simulations. As expected, the number of random coordinate generations decreases as both the donor and acceptor concentrations increase, since the amount of time spent checking for *D-D*, *D-A*, and *A-A* overlaps increases dramatically as more donors and acceptors are placed in the box.

The results of the simulations demonstrate excellent agreement between simulation and analytic theory, and also demonstrate the validity of assumptions (*a*) and (*d*) for physically reasonable values of the donor concentration, r_D, and r_A.

Effects of the Dipole-Dipole Orientation Factor

Up to this point, we have been purposefully vague in our discussion of the effects of the dipole-dipole orientation factor on the results previously derived. There are two reasons for this omission. First, Stryer (8) has demonstrated that in experiments where the *D* and *A* molecules possess some rotational mobility (e.g., a fluid phase bilayer [9, 10]), the uncertainty introduced into R_0 by the orientation factor is most probably no greater than 20%. Second, if assumption (*b*) holds, it is possible to calculate directly the effect of the orientation factor on Eq. 3 or 12.

As stated in assumption (*c*), there are two limits to consider. First, the orientation factor may be averaged on a time scale much shorter than the time scale of energy transfer (dynamic limit). Second, the orientation factor may be stationary in time for a given *D-A* pairing (static limit).

Let k in Eq. 3 be written as

$$k = \tau^{-1}\left\{1 + \sum_{i=1}^{N}\left[(<R_0>_d/R_i)^6(1.5\,\kappa_i^2)\right]\right\},$$

where $<R_0>_d$ is the dynamic average of R_0 over all orientations, and κ_i^2 is written in the form (3, 4)

$$\kappa_i^2 = [\sin\theta_D^{(i)}\sin\theta_{A_i}\cos\phi_{A_i} - 2\cos\theta_D^{(i)}\cos\theta_{A_i}] \tag{26}$$

(see Fig. 5).

TABLE II
COMPUTER SIMULATION OF FÖRSTER ENERGY TRANSFER

[*D*]	[*A*]	No. of coordinate generations*	Bad generations (overlaps)	q_r
			%	
0.1	0.01	1.99×10^5	0.93	0.961
0.5	0.01	6.99×10^4	5.81	0.962
0.1	0.05	1.62×10^5	0.98	0.823
0.5	0.05	6.23×10^4	6.35	0.831
0.1	0.09	1.36×10^5	0.92	0.712
0.5	0.09	5.61×10^4	5.66	0.725
0.1	0.30	7.13×10^4	1.40	0.352

*Computation time in all cases was 30 min for a Nova 840 computer (Data General Corp., Southboro, Mass.).

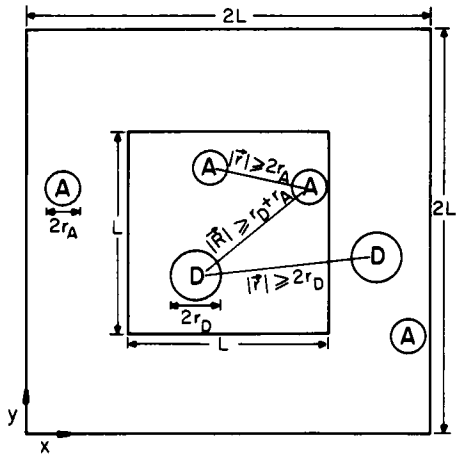

FIGURE 4

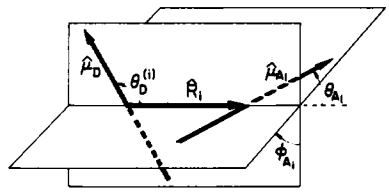

FIGURE 5

FIGURE 4 In a typical simulation, donors (D) and acceptors (A) with randomly generated x and y coordinates are placed in the large ($2L$) box, subject to the constraints indicated in the figure. The distances to all other donors and acceptors are checked. Three such distances and the conditions they must satisfy are shown above. **R** represents a vector involved in the energy transfer rate; **r** is used only to check constraints. When all donors and acceptors have been placed, $q_r^{(\phi)}$ is calculated, using only donors in the inner (L) box. In the above illustration, the donor and acceptor molecular radii r_D and r_A have been exaggerated for increased visibility. In a typical simulation, $L = 5\ R_0$, and $r_A = 0.05\ R_0$. In cases where r_D is not being varied, $r_D = 0.14\ R_0$. The simulation results are virtually independent of r_D and r_A for $r_D + R_A \leq 0.3\ R_0$.

FIGURE 5 μ_{A_i} and μ_D are unit vectors along with i^{th} acceptor absorption and donor emission transition dipoles, respectively. $\hat{R}_i$ is a unit vector along the vector joining the centers of μ_{A_i} and $\hat{\mu}_D$. θ_{A_i} and $\theta_D^{(i)}$ are peelback angles for $\hat{\mu}_{A_i}$ and $\hat{\mu}_D$ from $\hat{R}_i$, while ϕ_{A_i} is the dihedral angle between the planes formed by $\hat{\mu}_D$ and $\hat{R}_i$, and $\hat{\mu}_{A_i}$ and $\hat{R}_i$.

In the dynamic limit, a given D-A pair takes on all allowed orientations on a time scale short compared with τ. Therefore, k must be averaged over all possible values of κ_i^2. Since the A_i are independent, the averages over angles $\theta_D^{(j)}$, θ_{A_j}, and ϕ_{A_j}, $j \neq i$, are trivial and yield unity, while the average over $\theta_D^{(i)}$, θ_{A_i}, and ϕ_{A_i} is the same for any value of i, so that the dynamically averaged value of k, $<k>_d$ is given by

$$<k>_d = \tau^{-1}\left\{1 + \sum_{i=1}^{N} [\sigma_d^{1/6} <R_0>_d / R_i]^6\right\}$$

where

$$\sigma_d = (1.5) \int_0^{\pi} \int_0^{\pi} \int_0^{2\pi} \kappa^2\, \Phi_A(\phi_A)\, d\phi_A \circledR_A(\theta_A) \sin\theta_A d\theta_A \circledR_D(\theta_D) \sin\theta_D\, d\theta_D, \qquad (27)$$

and Φ_A, $\circledR_A$, and $\circledR_D$ are the normalized distribution functions for ϕ_A, θ_A, and θ_D, respectively. Note that when all orientations are possible with equal probability, $\sigma_d = 1$.

In the static limit, the averaging over orientations now takes place in the ensemble averaging of the decay function (4), so that Eq. 12 becomes

$$J(t) \approx 1 - \Gamma(2/2)\frac{\pi c \sigma_s <R_0>_d^2}{N}(t/\tau)^{1/3},$$

where

$$\sigma_s = (1.5)^{1/3}\int_0^{\pi}\int_0^{\pi}\int_0^{2\pi}(\kappa^2)^{1/3} \times \Phi_A(\phi_A)\,d\phi_A \circledR_A(\theta_A)\sin\theta_A d\theta_A \circledR_D(\theta_D)\sin\theta_D\,d\theta_D \quad (28)$$

and Φ_A, $\circledR_A$, and $\circledR_D$ are normalized distribution functions for static (rather than dynamic) angles.

In summary, the only change introduced by including the orientation factor is that in the dynamic limit R_0 becomes $\sigma_d^{1/6}<R_0>_d$, while in the static limit, R_0 becomes $\sigma_s^{1/2}<R_0>_d$, where σ_d and σ_s are given by Eqs. 27 and 28. The final effect of these changes is a scaling of the dimensionless concentration C. The inclusion of orientational effects has not, however, affected the functional form of $<P(t)>$. $<P(t)>$ will change form only if the orientation factor changes on a time scale comparable to τ.

DISCUSSION

The technique of Förster energy transfer in lipid bilayer membranes has recently been applied to several problems, including vesicle fusion (11), the structure of serum lipoproteins (12, 13), the distribution of lectin receptors on normal and transformed murine fibroblasts (14), the state of aggregation of Ca^{+2}-ATPase (15), and gramicidin (16) in reconstituted vesicles, and the determination of the surface density of labeled lipids in bilayers (1). We have recently applied the theory described in this paper to the quenching curves for the M13 coat protein tryptophan due to energy transfer to parinaric acid in dimyristoylphosphatidylcholine vesicles (17).

The theory presented above is applicable to two general kinds of structural questions. In the first case, specific donor-acceptor binding is of interest (15, 16) and the contribution of energy transfer between unassociated species must be known to determine association constants or stoichiometry. This application motivated another recent theoretical study (1). The second kind of application concerns the determination of the spatial parameter R_e, which is the minimum donor-acceptor distance. This may be the minimum lateral distance for donor-acceptor pairs at the same level in a bilayer or, as discussed below, it may be the vertical distance separating the two chromophores. This situation permits the application of this theoretical method to the determination of the depth of proteins in a membrane bilayer. An important aspect of the analytic treatment of this problem is that it permits us to examine the independence of the parameters extracted from quenching models and provides several guides to the design of quenching experiments.

It should be noted that, while the information contained in $<P(t)>$ and $q_r(C)$ is completely mathematically equivalent,[1] this equivalence assumes that R_0 is a known constant. As

[1]In general, this formalism produces relationships between $q_r(C)$ and $<P(t)>$ of the form $q_r(C) = \int_0^{\infty} e^{-\lambda}e^{-Cf(\lambda)}d\lambda$. This sort of integral equation is numerically invertible for a wide variety of functions $f(\lambda)$, and $<P(\lambda)> \propto e^{-\lambda}e^{-Cf(\lambda)}$.

previously stated, it will usually be the case that the value of R_0 computed from the spectral overlap of donor emission and acceptor absorption and the dynamic average value of κ^2 is reasonably close to the true value. However, if κ^2 is accidentally small, the result of using the dynamic average value of R_0 in computing C will be a quenching curve like the curves for large exclusion radius in Fig. 2. On the other hand, the curves in Fig. 2 may be made to coincide with the curve of Fig. 1 (within experimental error) by rescaling R_0. The results of such a rescaling are shown in Fig. 6. This calculation demonstrates that it is not possible to determine both R_0 and R_e from a static quenching experiment.

On the other hand, Fig. 7 shows that sets of parameters that give rise to the same relative quantum yield give very different decay curves, even given the noisiness of real data. Thus, the two parameters (R_e and R_0) needed to fit our most general model, the exclusion model, to a data set, are obtainable from two experiments, a quenching curve, and fluorescence lifetime experiment at some value of C. The values of R_0 and R_e that fit these data should then predict the fluorescence decay curve at any other value of C.

Eqs. 15 and 22 also provide another basis for distinguishing exclusion from an unfavorable value of R_0. The quenching curve for D-A pairs with smaller values of R_0 will be more

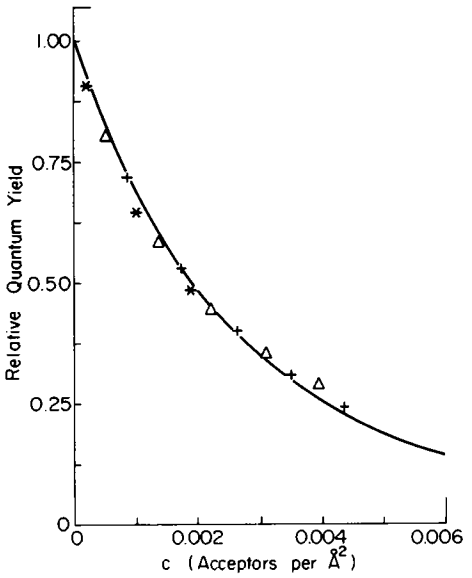

FIGURE 6

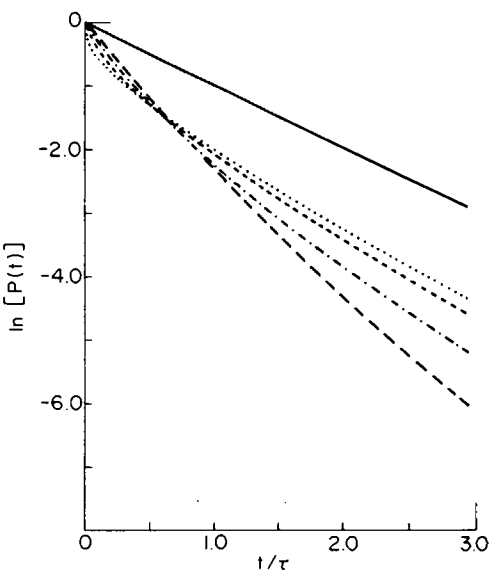

FIGURE 7

FIGURE 6 Values of q_r (as calculated by Eq. 22) for a given value of c (per Å^2) and varying values of R_e and R_0. The continuous curve (—) was generated for R_e = 0.0 Å, R_0 = 10.0 Å. The plotted points were then generated by fixing R_e/R_0 and varying R_0 until q_r was the same as that for the R_e = 0.0 case at the same value of c. Points shown are for R_0 = 11.7 Å, R_e = 6.5 Å(+); R_0 = 15.3 Å, R_e = 12.2 Å(△); R_0 = 22.2 Å, R_e = 23.3 Å(∗).

FIGURE 7 Fluorescence decay curves for the values of R_e and R_0 used in Fig. 6, as calculated by Eq. 21. The curve for c = 0.0 Å^{-2} (—) is presented for reference. For all other curves, c = 2.4 × 10^{-3} Å^{-2}. The curves shown are for R_0 = 10.0 Å, R_e = 0.0 Å (....); R_0 = 11.7 Å, R_e = 6.5 Å (---); R_0 = 15.3 Å, R_e = 12.2 Å (·---·); R_0 = 22.2 Å, R_d = 23.3 Å (---). All of the decays, except the c = 0.0 Å^{-2} curve, yield q_r = 0.42. This corresponds to a value of c such that, when t/τ = 1, the R_e = 0.0 curve has dropped by a factor of e^{-2}.

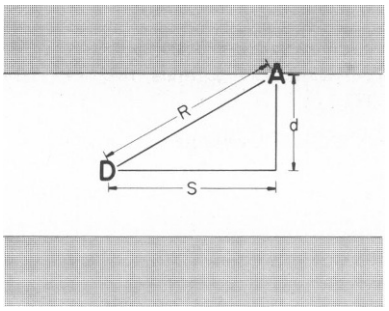

FIGURE 8 Donor and acceptor at different levels in the membrane. Since $R^2 = S^2 + d^2$ and $W(R)\mathrm{d}R \propto W(S)\mathrm{d}S$, $W(R)\mathrm{d}R = 2R\mathrm{d}R/(R_d^2 - d^2)$, which is the same as the form used to derive Eqs. 21 and 22, if $R_e = d$.

sensitive to exclusion radius effects, since R_e/R_0 will be larger for such pairs. If the donor or acceptor molecule's spectroscopic characteristics can be changed without changing the distribution, the orientation factor, or the exclusion radius, R_e, comparison of quenching data from several *D-A* pairs will permit determination of both R_0 and R_e.

The treatment leading to Eq. 23 and Fig. 3 demonstrates the well-known and important fact that the quenching curve in the case of *D-A* binding depends markedly on donor concentration. Eq. 23 also demonstrates that in two dimensions the contribution of random quenching to the total quenching can be significant even if all of the quenchers are bound to donors.

The case of donors and acceptors at different levels in the bilayer, depicted in Fig. 8, is mathematically the same as the case for exclusion with $R_e = d$, if κ^2 undergoes enough dynamic or static averaging that assumption (*b*) is still approximately true.

Finally, the comparison of analytic and computer simulation results provides a check on the accuracy of both techniques, given the assumptions they hold in common. The degree of agreement indicated by Figs. 1–3 is far better than noise associated with most experiments, indicating that an experimentalist is safe using either approach to interpret real data. However, the computational speed of the analytic theory, along with the provision for computing functional forms of decay curves as well as quenching curves, will probably make the analytic theory more useful in interpreting real data.

CONCLUSION

The analytic solution of the random Förster energy transfer problem in two dimensions provides a basis for evaluating the experimental utility of this technique. The expression of model parameters as dimensionless numbers is a simple but essential step towards making the problem tractable. The results derived in this paper should be useful in the interpretation of experiments designed to measure lipid head group areas, bilayer thicknesses, exclusion phenomena, vesicle fusion, and binding characteristics by means of random Förster transfer in bilayer membrane systems.

Acknowledgment is given to Lubert Stryer for providing the results of his numerical simulation of the problem, to Lubert Stryer and Bernard Fung for providing a preprint of their experimental study of two-dimensional energy

transfer, to Dave Thomas for discussions of the effect of diffusion on energy transfer, and to Larry Sklar for discussions on the behavior of donors and acceptors at different levels in a bilayer membrane.

This work was supported by U. S. Public Health Service grants GM21149 and EY01518. Dr. Hudson is a Research Career Development awardee (GM00284).

Received for publication 6 November 1978 and in revised form 30 April 1979.

REFERENCES

1. FUNG, B. K., and L. STRYER. 1978. Surface density determination in membranes by fluorescence energy transfer. *Biochemistry.* **17**:5241.
2. FÖRSTER, T. 1949. Experimentelle und theoretische Untersuchung des zwischenmolekularen Übergangs von Elektronenanregungsenergie. *Z. Naturforsch. A. Astrophys. Phys. Phys. Chem.* **4**:321.
3. EISENTHAL, K. B., and S. SIEGEL. 1964. Influence of resonance transfer on luminescence decay. *J. Chem. Phys.* **41**:652.
4. DALE, R. E., and J. EISINGER. 1975. Polarized excitation energy transfer. *In* Biochemical Fluorescence: Concepts, VI. R. F. Chen and H. Edelhock, editors. Marcel Dekker, Inc., New York. 120.
5. TWEET, A. G., W. D. BELLAMY, and G. L. GAINES, Jr. 1964. Fluorescence quenching and energy transfer in monomolecular films containing chlorophyll. *J. Chem. Phys.* **41**:2068.
6. HAUSER, M., U. K. A. KLEIN, and U. GÖSELE. 1976. Extension of Förster's theory of long range energy transfer to donor-acceptor pairs in systems of molecular dimensions. *Z. Phys. Chem.* **101**:255.
7. DAVIS, P. J., and I. POLONSKI. 1964. Numerical interpolation, differentiation and integration. *In* Handbook of Mathematical Functions. M. Abramowitz and I. A. Stegun, editors. National Bureau of Standards applied mathematics series. 923.
8. STRYER, L. 1978. Fluorescence energy transfer as a spectroscopic ruler. *Annu. Rev. Biochem.* **47**:819.
9. KAWATO, S., K. KINOSITA, and A. IKEGAMI. 1977. Dynamic structure of lipid bilayers studied by nanosecond fluorescence techniques. *Biochemistry.* **16**:2319.
10. CHEN, L. A., R. E. DALE, and L. BRAND. 1977. Nanosecond time-dependent depolarization of diphenylhexatriene in dimyristoyllecithin vesicles and the determination of "microviscosity." *J. Biol. Chem.* **252**:2163.
11. VAN DER WERF, P., and E. F. ULLMAN. 1979. Measurement of liposome fusion by energy transfer fluorescence quenching. *Fed. Proc.* **38**:459.
12. SKLAR, L. A., M. C. DOODY, A. M. GOTTO, Jr., and H. J. POWNALL. 1979. Fluorescence energy transfer localization of probes, lipids and protein in serum lipoproteins. *Biophys. J.* **25**:285*a*. (Abstr.)
13. DOODY, M. C., L. A. SKLAR, H. J. POWNALL, J. T. SPARROW, and A. M. GOTTO, Jr., and L. C. SMITH. 1979. Models for fluorescence energy transfer in serum lipoproteins, lipoprotein complexes and membranes. *Biophys. J.* **25**:286*a*. (Abstr.)
14. FERNANDEZ, S. M., and R. D. BERLIN. 1976. Cell surface distribution of lectin receptors determined by resonance energy transfer. *Nature (Lond.).* **264**:411.
15. VANDERKOOI, J. M., A. IEROKOMAS, H. NAKAMURA, and A. MARTONOSI. 1977. Fluorescence energy transfer between Ca^{+2} transport ATPase molecules in artificial membranes. *Biochemistry.* **16**:1262.
16. VEATCH, W., and L. STRYER. 1977. The dimeric nature of the gramicidin A transmembrane channel: conductance and fluorescence energy transfer studies of hybrid channels. *J. Mol. Biol.* **113**:89.
17. KIMELMAN, D., E. S. TECOMA, P. K. WOLBER, B. S. HUDSON, W. T. WICKNER, and R. D. SIMONI. 1979. Protein-lipid interactions: studies of the M13 coat protein in dimyristoylphosphatidylcholine vesicles using parinaric acid. *Biochemistry.* In press.